TURBULENT CHANNEL FLOW WITH STREAMWISE ROTATION: LIE GROUP ANALYSIS, DNS AND MODELING

Martin Oberlack
Institut für Technische Mechanik, RWTH Aachen, 52056 Aachen, Germany

William H. Cabot
Center for Turbulence Research, Stanford University, Stanford, CA 94305-3030, USA

Michael M. Rogers
Center for Turbulence Research, NASA/Ames Research Center, CA 94035-1000, USA

ABSTRACT

The turbulent channel flow with streamwise rotation has been investigated by means of different analytical, numerical, and modeling approaches. Lie group analysis of the two-point correlation equations led to linear scaling laws for the streamwise mean velocity. In addition it was found that a cross flow in spanwise direction is induced, which may also exhibit a linear region. It is shown that all six components of the Reynolds stress tensor are non-zero. In addition certain symmetries about the centerline have been established for all flow quantities. All the latter findings of the analysis have been very well verified by means of direct numerical calculations. The flow has also been tackled by LES and second-moment closure models. The dynamic LES model captured most of the theoretical and DNS findings quantitatively. The second-moment closure model was able to capture most of the basic trends, but any quantitative agreement could not be achieved.

INTRODUCTION

During the development of the symmetry theory in Oberlack (1997), it was noticed that there may be one additional turbulent scaling law which was not mentioned since no experimental or DNS data were available. This is the turbulent channel flow rotating about the streamwise direction (see Fig. 1).

The classical rotating turbulent channel flow considers rotation about the spanwise direction (x_3) (Johnston *et al.* 1972). In this flow the mean stream lines follow plane spirals. In contrast to this, mean stream lines of the present flow exhibit corkscrew-like spirals. However, the most obvious difference between the two cases may be the induction of a cross flow in x_3-direction.

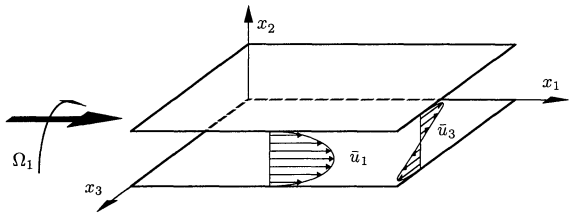

FIGURE 1. Sketch of the flow geometry of a turbulent channel flow with streamwise rotation.

ANALYSIS

The basis for the flow analysis the present section is the mean momentum equation and the two-point velocity correlation equation in a rotating frame of reference, which are given respectively by

$$0 = -\frac{1}{\rho}\frac{\partial \bar{p}}{\partial x_1} - \frac{\partial \overline{u_1 u_2}}{\partial x_2} + \nu \frac{\partial^2 \bar{u}_1}{\partial x_2^2} \ , \tag{1}$$

$$0 = -\frac{1}{\rho}\frac{\partial \bar{p}}{\partial x_2} - \frac{\partial \overline{u_2 u_2}}{\partial x_2} - 2\,\Omega_1 \bar{u}_3 \ , \tag{2}$$

$$0 = -\frac{\partial \overline{u_2 u_3}}{\partial x_2} + \nu \frac{\partial^2 \bar{u}_3}{\partial x_2^2} \tag{3}$$

and

$$\begin{aligned} 0 = & -R_{2j}\delta_{i1}\frac{\mathrm{d}\bar{u}_1(x_2)}{\mathrm{d}x_2} - R_{2j}\delta_{i3}\frac{\mathrm{d}\bar{u}_3(x_2)}{\mathrm{d}x_2} \\ & - R_{i2}\delta_{j1}\frac{\mathrm{d}\bar{u}_1(x_2+r_2)}{\mathrm{d}(x_2+r_2)} - R_{i2}\delta_{j3}\frac{\mathrm{d}\bar{u}_3(x_2+r_2)}{\mathrm{d}(x_2+r_2)} \\ & - [\bar{u}_1(x_2+r_2) - \bar{u}_1(x_2)]\,\frac{\partial R_{ij}}{\partial r_1} \\ & - [\bar{u}_3(x_2+r_2) - \bar{u}_3(x_2)]\,\frac{\partial R_{ij}}{\partial r_3} \\ & - \frac{1}{\rho}\left[\delta_{i2}\frac{\partial \overline{pu_j}}{\partial x_2} - \frac{\partial \overline{pu_j}}{\partial r_i} + \frac{\partial \overline{u_i p}}{\partial r_j}\right] \end{aligned}$$

$$+\nu\left[\frac{\partial^2 R_{ij}}{\partial x_2 \partial x_2} - 2\,\frac{\partial^2 R_{ij}}{\partial x_2 \partial r_2} + 2\,\frac{\partial^2 R_{ij}}{\partial r_k \partial r_k}\right]$$
$$-\frac{\partial R_{(i2)j}}{\partial x_2} + \frac{\partial}{\partial r_k}\left[R_{(ik)j} - R_{i(jk)}\right]$$
$$-2\,\Omega_1\left[e_{1li}R_{lj} + e_{1lj}R_{il}\right] \ . \qquad (4)$$

$\bar{u}_i$, $\bar{p}$, $\overline{u_i u_j}$, ν, and Ω_1 are respectively the mean velocity, the mean pressure, the Reynolds stress tensor, the dynamic viscosity, and the rotation rate in x_1-direction. The two-point velocity correlation tensor function and the two-point pressure-velocity in Eq. (4) are respectively defined as

$$R_{ij}(\boldsymbol{x}, \boldsymbol{r}; t) = \overline{u_i(\boldsymbol{x}, t)\, u_j(\boldsymbol{x}^{(1)}, t)} \ ,$$
$$\overline{pu_j}(\boldsymbol{x}, \boldsymbol{r}; t) = \overline{p(\boldsymbol{x}, t)\, u_j(\boldsymbol{x}^{(1)}, t)} \qquad (5)$$

where u_i and p are the fluctuating quantities. The other tensors are defined accordingly. For the present case all statistical quantities only depend on the wall-normal coordinate x_2 and the correlation coordinate $\boldsymbol{r} = \boldsymbol{x}^{(1)} - \boldsymbol{x}$. The double two-point correlation tensor R_{ij} converges to the Reynolds stress tensor $\overline{u_i u_j}$ in the limit of zero separation $|\boldsymbol{r}| = 0$.

For high Reynolds number flows, viscous transport terms are only significant in the very vicinity of the wall. From Eq. (1) the usual linear turbulent shear stress profile for $\overline{u_1 u_2}$ may be derived. Since no pressure-gradient in the spanwise (x_3) direction is present, it can be deduced from Eq. (3) that the shear stress $\overline{u_2 u_3}$ is uniform. Equation (2) only determines the pressure-gradient in wall-normal direction and has no influence on the mean velocity.

Time-scale analysis

The characteristic time scales of the rotation rate the viscous sublayer and the universal logarithmic region are respectively defined as

$$t_\Omega \equiv \frac{1}{\Omega_1} \ , \ t_\nu \equiv \frac{\nu}{u_\tau^2} \quad \text{and} \quad t_{\log} \equiv \frac{y}{u_\tau} \qquad (6)$$

where u_τ is the "friction velocity" defined as $u_\tau = \sqrt{\nu \left.\frac{\partial \bar{u}_1}{\partial x_2}\right|_{\text{wall}}}$. For sufficiently high Reynolds number, t_ν is a fixed small quantity while $t_{\log}$ increases with the distance from the wall. Taking the ratio of the latter flow time scales with the rotation time scale we respectively obtain

$$T_1 = \frac{t_\nu}{t_\Omega} = \frac{\nu\Omega_1}{u_\tau^2} = \frac{\text{Ro}}{2\text{Re}} \qquad (7)$$

and

$$T_2 = \frac{t_{\log}}{t_\Omega} = \frac{y\Omega_1}{u_\tau} = \text{Ro}\frac{y}{h} \ , \qquad (8)$$

where $\text{Re} = hu_\tau/2\nu$ and $\text{Ro} = \Omega_1 h/u_\tau$.

Assuming Ro of the order $O(1)$ and supposing Re to be large, the time scale ratio T_1 is a small quantity. Hence it is concluded that the rotation only perturbs the viscous sublayer, and a significant change may not be observed.

Considering the same order of magnitude assumptions for Ro as above, it can be concluded that T_2 may only be a small parameter for small y/h. This is the flow region close to the wall and next to the viscous sublayer. In contrast, if y/h is of order $O(1)$, T_2 may become an order $O(1)$ parameter. Consequently, we conclude that this is the flow region which is affected most by the system rotation as will be shown subsequently.

Reflection symmetries about the centerline

The following is observed in a variety of different channel type of flows such as the usual turbulent Poiseuille and the turbulent Couette flow: If the corresponding equations and boundary conditions admit a certain reflection symmetry about the centerline, this is also verified for all statistical quantities.

For the present problem the system (1)-(4) admits a reflection symmetry where the variables are respectively separated as independent variables, mean quantities, and statistical quantities

$$\tilde{x}_1 = x_1 \ , \ \tilde{x}_2 = -x_2 \ , \ \tilde{x}_3 = -x_3 \ , \qquad (9)$$
$$\tilde{r}_1 = r_1 \ , \ \tilde{r}_2 = -r_2 \ , \ \tilde{r}_3 = -r_3 \ , \qquad (10)$$
$$\tilde{\bar{u}}_1 = \bar{u}_1 \ , \quad \tilde{\bar{u}}_3 = -\bar{u}_3 \ , \quad \tilde{\bar{p}} = \bar{p} \qquad (11)$$

and

$$\begin{pmatrix} \tilde{R}_{11} & \tilde{R}_{12} & \tilde{R}_{13} \\ \tilde{R}_{21} & \tilde{R}_{22} & \tilde{R}_{23} \\ \tilde{R}_{31} & \tilde{R}_{32} & \tilde{R}_{33} \end{pmatrix} = \begin{pmatrix} R_{11} & -R_{12} & -R_{13} \\ -R_{21} & R_{22} & R_{23} \\ -R_{31} & R_{32} & R_{33} \end{pmatrix} \ . \qquad (12)$$

The latter reflection symmetries can be generalized as such that any other statistical quantity can be determined from the fluctuation quantities according to the transformation for the fluctuations

$$\tilde{u}_1 = u_1 \ , \quad \tilde{u}_2 = -u_2 \ , \quad \tilde{u}_3 = -u_3 \ , \quad \tilde{p} = p \ . \qquad (13)$$

For example, the transformation (12) can be determined from (13) as a dyadic product. Employing (9)-(13) and the corresponding quantities in the statistical transport equations do not change its form written in the "~"-quantities.

From (11) it can be determined that $\bar{u}_1$ is symmetric about the centerline and $\bar{u}_3$ is antisymmetric about the centerline. The consequences for the stresses are such that all normal stresses and $\overline{u_2 u_3}$ are symmetric about the centerline while $\overline{u_1 u_2}$ and $\overline{u_1 u_3}$ are antisymmetric about the centerline.

Lie group analysis of the correlation equation

In the following analysis it will be assumed that the Reynolds number tends to infinity so that the viscous terms in the two-point correlation equation (4) may be neglected. The basis for this assumption is the fact that, to leading order only, the large scales determine the mean velocity. Viscosity only affects the small scales of the order $O(\eta)$ where η is the Kolmogorov length scale. Hence neglecting viscosity is only valid for $|\boldsymbol{r}| \gg \eta$. If $|\boldsymbol{r}| \ll \eta$, the last term of the third line in Eq. (4) corresponds to the dissipation and cannot be neglected.

The general purpose of the present analysis is to achieve self-similarity (or reduction) of the two-point correlation equation and to find analytical solutions for

the mean velocity. The first step to accomplish this objective is to find continuous symmetry transformations (Lie groups). In fact, this is analogous to the analysis presented in the previous subsection where reflection symmetries have been investigated which do not alter the equations. The method to find the desired continuous groups of transformations is called Lie group analysis (see e.g. Bluman and Kumei 1989). In the present subsection only a heuristic approach will be presented while some more mathematical details on group methods are presented in Appendix B in Oberlack (1997).

Self-similarity or reduction is always associated with the decrease of the number of independent variables. It is important to note that the independent variables are not necessarily restricted to the usual variables such as $\boldsymbol{x}$ and t. Instead any parameter in the equation under investigation may be considered as independent variable.

Hence, in the first step a reduction will be achieved by rewriting the two-point correlation equation as such that Ω_1 is absorbed into all the remaining independent and dependent variables. The most general form of transformation allowing this reduction is

$$x_i = \tilde{x}_i\gamma(\Omega_1),\ \ r_i = \tilde{r}_i\gamma(\Omega_1),\ \ \bar{u}_i = \tilde{\bar{u}}_i\gamma(\Omega_1)\Omega_1,$$
$$R_{ij} = \tilde{R}_{ij}\gamma(\Omega_1)^2\Omega_1^2\ ,\ \ \overline{pu}_i = \widetilde{\overline{pu}}_i\gamma(\Omega_1)^3\Omega_1^3\ , \qquad (14)$$

where the new variables are denoted by tilde, and $\gamma(\Omega_1)$ is an arbitrary function of Ω_1. After employing (14) and imposing the high Reynolds number limit in (4), the two-point correlation equations have a similar form as (4) but the viscous term has disappeared and Ω_1 is no longer contained in the equation.

Obviously the number of elements in the vector of independent variables $[r_1, r_2, r_3, x_2, \Omega_1]$ has been reduced by one. From the Lie group approach in Oberlack (1997) it follows that the latter equation admits a further similarity reduction only for certain mean velocities which obey the equations

$$[a_1\tilde{x}_2 + a_2]\frac{\mathrm{d}\tilde{\bar{u}}_1(\tilde{x}_2)}{\mathrm{d}\tilde{x}_2} - a_1\tilde{\bar{u}}_1(\tilde{x}_2) = c_1\ , \qquad (15)$$

$$[a_1\tilde{x}_2 + a_2]\frac{\mathrm{d}\tilde{\bar{u}}_3(\tilde{x}_2)}{\mathrm{d}\tilde{x}_2} - a_1\tilde{\bar{u}}_3(\tilde{x}_2) = c_3 \qquad (16)$$

where a_1, a_2, c_1 and c_3 are constants. The corresponding similarity variables for the correlation functions are to be obtained from the invariant surface condition

$$\frac{d\tilde{r}_1}{a_1\tilde{r}_1} = \frac{d\tilde{r}_2}{a_1\tilde{r}_2} = \frac{d\tilde{r}_3}{a_1\tilde{r}_3}$$
$$= \frac{d\tilde{x}_2}{a_1\tilde{x}_2 + a_2} = \frac{d\tilde{R}_{ij}}{2a_1\tilde{R}_{ij}} = \frac{d\widetilde{\overline{pu}}_i}{3a_1\widetilde{\overline{pu}}_i} \qquad (17)$$

where the constants of integration are taken as the new variables.

Each of the parameters a_1 and a_2 have a distinct physical meaning. The parameter a_1 corresponds to the scaling group; i.e. Eq. (4) admits a transformation of the form

$$\tilde{x}_2^* = \mathrm{e}^{a_1}\tilde{x}_2\ ,\quad \tilde{r}_i^* = \mathrm{e}^{a_1}\tilde{r}_i\ ,\quad \tilde{\bar{u}}_i^* = \mathrm{e}^{a_1}\tilde{\bar{u}}_i\ , \qquad (18)$$

$$\tilde{R}_{ij}^* = \mathrm{e}^{2a_1}\tilde{R}_{ij}\ ,\quad \widetilde{\overline{pu}}_i^* = \mathrm{e}^{3a_1}\widetilde{\overline{pu}}_i\ , \qquad (19)$$

which does not alter the functional form of the equation written in the new coordinates. The parameter a_2 corresponds to the translation group which conform to the fact that (4) is autonomous with respect to $\tilde{x}_2$. As a result (4) is invariant under the transformation

$$\tilde{x}_2^* = \tilde{x}_2 + a_2\ . \qquad (20)$$

The equations (15) and (16) integrate to

$$\tilde{\bar{u}}_1 = C_1\left(\tilde{x}_2 + \frac{a_2}{a_1}\right) - \frac{c_1}{a_1}\ ,$$
$$\tilde{\bar{u}}_3 = C_3\left(\tilde{x}_2 + \frac{a_2}{a_1}\right) - \frac{c_3}{a_1}\ , \qquad (21)$$

where C_1 and C_3 are integration constants. If the transformation (14) to the original coordinates is inferred, the latter equations read

$$\bar{u}_1 = C_1\,\Omega_1\,x_2 + \Omega_1\,\gamma(\Omega_1)\left(C_1\frac{a_2}{a_1} - \frac{c_1}{a_1}\right)\ ,$$
$$\bar{u}_3 = C_3\,\Omega_1\,x_2 + \Omega_1\,\gamma(\Omega_1)\left(C_3\frac{a_2}{a_1} - \frac{c_3}{a_1}\right)\ . \qquad (22)$$

Though a solid theoretical basis on first principles is still lacking, it appears that to leading order the two-point correlation function does not scale with the rotation rate Ω_1. Hence it can be concluded from Eq. (14) that, in order to have no Ω_1 dependence of R_{ij}, the function γ behaves as $\gamma \sim 1/\Omega_1$. As a result, the two additive constants appearing in the scaling laws (22) do not depend on Ω_1 either. Only the slope of the linear scaling laws depends on the rotation rate.

The similarity variables corresponding to the mean velocity (22) are to be obtained from the characteristic Eqs. (17). The integration yields

$$\eta_i = \frac{\tilde{r}_i}{\tilde{x}_2 + \frac{a5}{a_1}}\ ,\quad \tilde{R}_{ij} = F_{ij}\left(\tilde{x}_2 + \frac{a_2}{a_1}\right)^2\ ,$$
$$\widetilde{\overline{pu}}_i = G_i\left(\tilde{x}_2 + \frac{a_2}{a_1}\right)^3\ , \qquad (23)$$

where the integration constants η_i, F_{ij} and G_i are the new similarity variables. In order to verify the similarity reduction of Eq. (4) (in the limit $\nu \to 0$), the quantities F_{ij} and G_i are introduced as new dependent variables only depending on η_i.

It should be noted that the presented results are not limited to the two-point correlation equation only. Indeed all results are consistent with correlation equations up to any arbitrary order. Due to space restrictions this has not been shown here.

DIRECT NUMERICAL SIMULATION

A DNS of the rotating channel flow has be conducted. The utilized boundary conditions and the spectral method is the same as in Kim *et al.* (1987). The flow quantities are non-dimensionalized by $h/2$ and u_τ

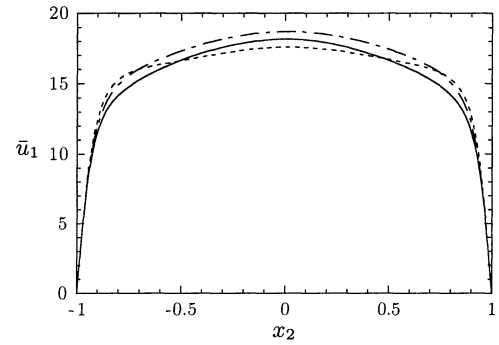

FIGURE 2. Streamwise mean velocity at Ro = 0 ——— , Ro = 3.2 — - — and Ro = 10 — — — .

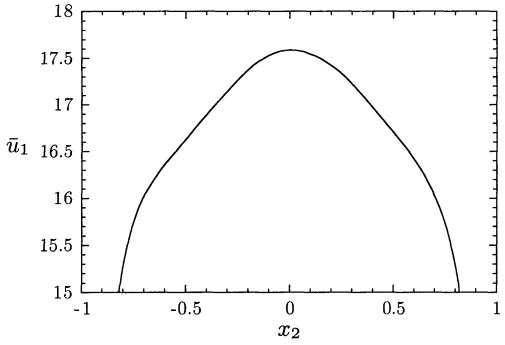

FIGURE 3. Streamwise mean velocity at Ro = 10 in the core region.

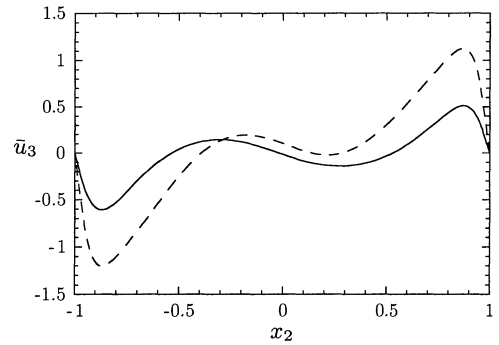

FIGURE 4. Spanwise mean velocity at Ro = 3.2 ——— and Ro = 10 — — — .

where h is the channel width and u_τ is the friction velocity of the non-rotating case. The density ρ is set to unity. The rotation number and the Reynolds number with its numerical value for all subsequent calculations below are respectively

$$\mathrm{Ro} = \frac{\Omega_1 h}{u_\tau} \quad \text{and} \quad \mathrm{Re}_\tau = \frac{h u_\tau}{2\nu} = 180 \ . \qquad (24)$$

Two computations at rotation numbers of Ro = 3.2 and Ro = 10 have been conducted. All presented results for Ro = 0 have been taken from Kim *et al.* (1987). The domain size and the grid is to be obtained from Oberlack *et al.* (1998). In Fig. 2 the streamwise mean

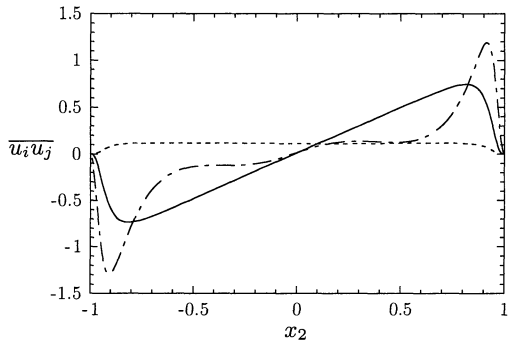

FIGURE 5. Shear stresses at Ro = 10: $\overline{u_1 u_2}$ ——— , $\overline{u_2 u_3}$ — — — , $\overline{u_1 u_3}$ — - — .

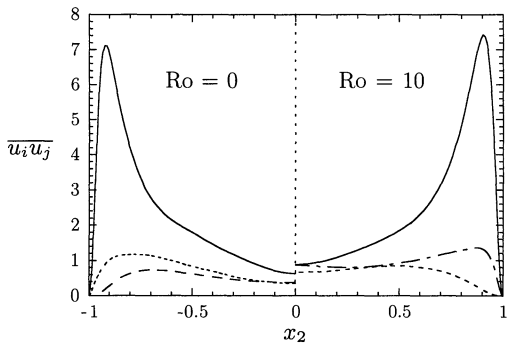

FIGURE 6. Normal stresses at Ro = 0 and Ro = 10: $\overline{u_1 u_1}$ ——— , $\overline{u_2 u_2}$ — — — , $\overline{u_3 u_3}$ — - — .

velocity profiles at Ro = 0, Ro = 3.2, and Ro = 10 are compared. As expected from the time scale analysis, the near-wall region up to $x_2 = \pm 0.9$ is only marginally perturbed. Approaching the core region of the flow, a significant change in the mean velocity profile is visible with a very pronounced shoulder at $x_2 = \pm 0.8$ for Ro = 10. In addition, a much flatter center region is noticeable. For the lower rotation rate no linear region is noticeable.

As predicted by the group analysis, two linear regions emerge on each side of the centerline for the high rotation rate. A more detailed perspective of the linear region is given in Fig. 3 where only the "head" of the profile for Ro = 10 is depicted. The linear regions cover the wide range $x_2 = 0.2 - 0.6$ on both sides of the center line.

As already mentioned previously, a mean cross flow denoted by $\bar{u}_3$ is induced by the rotation. It was prognosticated that the flow is skew-symmetric about the centerline as shown in Fig. 4.

Though a still clearer verification is still lacking, it appears that the predicted linear profile is also visible in the induced crossflow. The location of the linear region is slightly shifted towards the wall region compared to the linear region of the streamwise velocity. An interesting feature of the cross flow is the region near the centerline. Therein the cross flow has opposite

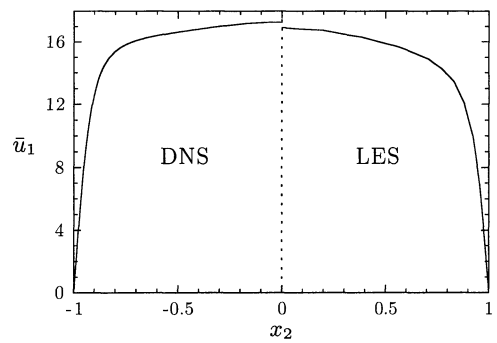

FIGURE 7. Streamwise mean velocity from DNS on the left- and LES on the right-hand side at Ro = 10.

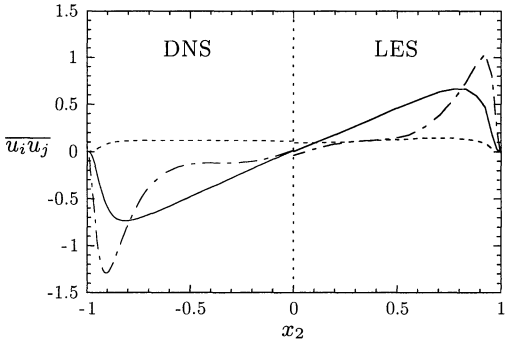

FIGURE 8. Shear stresses from DNS and LES at Ro = 10: $\overline{u_1u_2}$ ———, $\overline{u_2u_3}$ – – –, $\overline{u_1u_3}$ — - —.

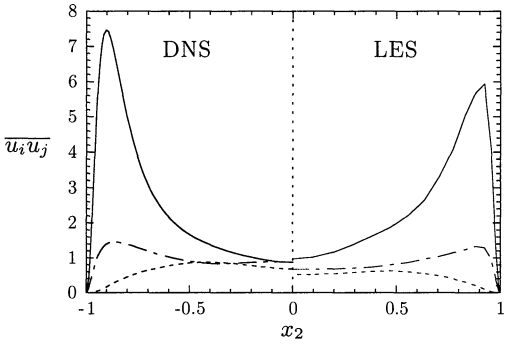

FIGURE 9. Normal stresses from DNS and LES at Ro = 10: $\overline{u_1u_1}$ ———, $\overline{u_2u_2}$ – – –, $\overline{u_3u_3}$ — - —.

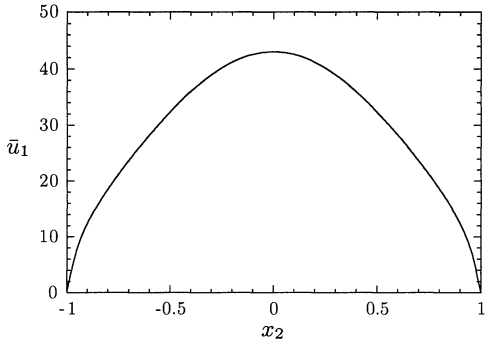

FIGURE 10. Streamwise velocity from the RANS model at Ro = 28.

sign compared to the flow regions closer to the channel walls.

In Fig. 5 the Reynolds shear stresses at Ro = 10 are displayed. Both the linear and the constant curves for $\overline{u_1u_2}$ and $\overline{u_2u_3}$ respectively can be derived from the Eqs. (1) and (3) by neglecting the viscous terms. One of the most intriguing features of the shear stresses is the induced $\overline{u_1u_3}$ component. The two other cross stresses can both be interpreted in terms of a simplified eddy-viscosity type of sense from its corresponding mean velocities. However, this cannot be done for the $\overline{u_1u_3}$ shear stress. Hence $\overline{u_1u_3}$ can only be modeled with the aid of more elaborate turbulence models such as LES or Reynolds stress transport models, to be presented in the next subsection.

The normal stresses for both the rotating and the non-rotating case are depicted in Fig. 6. Obviously, only very weak differences are noticeable compared to the strong change in the mean streamwise mean velocity induced by the rotation.

LES AND SECOND-MOMENT CLOSURE MODELS

Classical two-equation models such as the k-ε or the k-ω model have not been examined since they exhibit no reaction on system rotation at all.

The first turbulence model to be investigated is the dynamic subgrid-scale model (Germano *et al.* 1991) used in LES. The flow parameters and the numerical scheme are the same as for the DNS. The grid sizes are to be taken from Oberlack *et al.* (1998).

In Fig. 7 the streamwise mean velocities from DNS and LES are compared. Even though the LES profile changes significantly due to the system rotation it does not exhibit a clear linear region as was observed in the DNS. In addition, the mass flux is marginally smaller.

In Fig. 8 and 9 the shear and the normal stresses from the DNS are very well represented by the LES calculation.

The second turbulence model to be applied to the present type of flow is a second-moment closure model. The equations are based on the IP model (see Launder *et al.* 1975) and the SSG model (see Speziale *et al.* 1989). The near-wall behavior of the pressure-strain term is modeled by the elliptic-relaxation approach developed by Durbin (1991). Model parameters have been taken from the original publications.

The turbulent diffusion terms have a very strong influence on the model results. Hence the linear regions in the streamwise velocity are only visible at very high rotation rates for which DNS results have not been obtained yet. In Fig. 10 the streamwise velocity is shown for the very high rotation number Ro = 28 obtained with the IP model.

Besides the usual Coriolis terms, the rotation rate Ω_1 only appears in the pressure-strain model. Since the

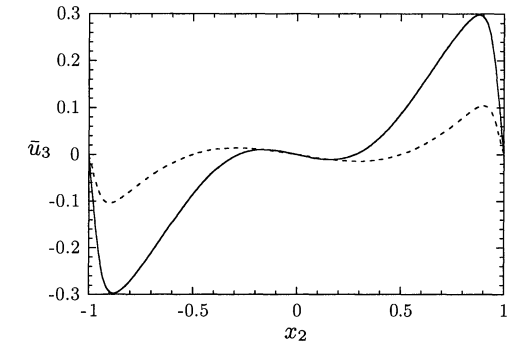

FIGURE 11. Spanwise velocity from the RANS model at Ro = 3.2: IP model ——— , SSG model – – – .

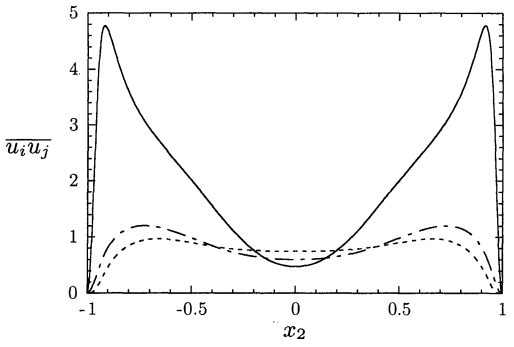

FIGURE 12. Normal stresses from the SSG model at Ro = 10: $\overline{u_1u_1}$ ——— , $\overline{u_2u_2}$ – – – , $\overline{u_3u_3}$ — - — .

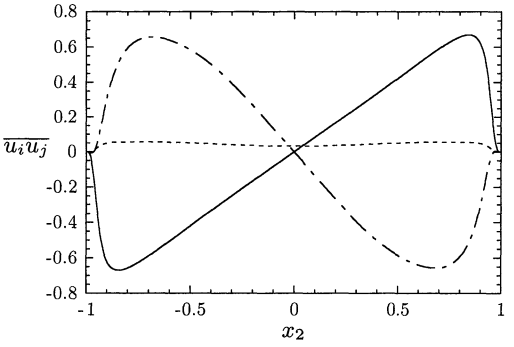

FIGURE 13. Shear stresses from the SSG model at Ro = 10: $\overline{u_1u_2}$ ——— , $\overline{u_2u_3}$ – – – , $\overline{u_1u_3}$ — - — .

cross flow and the stress components $\overline{u_2u_3}$ and $\overline{u_1u_3}$ are solely induced by the rotation, it is the pressure-strain model in particular which determines these quantities. As a result the cross flow is extremely sensitive to the implemented pressure-strain model. In Fig. 11 the spanwise velocities for the IP and the SSG model are compared at Ro = 3.2. Apparently the shape of the DNS curve in Fig. 5 is represented by both models. Much less sensitive to the pressure-strain model are the normal stresses. In Fig. 12 the normal stress from the SSG model are presented which are within 30% of the DNS results.

In contrast to this, it can be seen in Fig. 13 that from the shear stresses only $\overline{u_1u_2}$ is obtained with reasonable agreement. Though an almost constant $\overline{u_2u_3}$ component is obtained in the center region of the flow as predicted by the DNS, its value is much too small. The $\overline{u_1u_3}$ is not even qualitatively correct. The sign of $\overline{u_1u_3}$ disagrees with the result from the DNS.

SUMMARY AND CONCLUSIONS

The general purpose of the present work is to establish a new but still very simple canonical test case to study basic turbulence physics. It has been confirmed by DNS that there are linear regions in both the streamwise and the spanwise mean velocity as was suggested by Lie group analysis of the two-point correlation equations. Beside the mean flow, all six Reynolds stress quantities have been computed. The stress components from the DNS have the expected symmetry properties about the centerline as predicted by the symmetry analysis.

A LES computation has been conducted which captures most of the DNS results very well. Only the linear regions in the streamwise velocity were not clearly visible. Employing a second-moment model, some basic trends of the flow have been captured. However quantitative agreement was not achieved and the results where very sensitive to the pressure-strain model.

REFERENCES

Bluman, G. W. & Kumei, S., 1989, "Symmetries and Differential Equations", Springer.

Durbin, P., 1991, "Near-wall turbulence closure modeling without 'damping functions'", *Theoret. Comput. Fluid Dyn.*, Vol. 3, pp. 1-13.

Germano, M., Piomelli, U., Moin, P., & Cabot, W. H., 1991, "A dynamic subgrid-scale eddy viscosity model", *Phys. Fluids A*, Vol. 3, pp. 1760-1765.

Johnston, J. P., Halleen, R. M. & Lazius, D. K., 1972, "Effects of spanwise rotation on the structure of two-dimensional fully developed turbulent channel flow", *J. Fluid Mech*, Vol. 56, pp. 533-557.

Kim, J., Moin, P. & Moser, R., 1987, "Turbulence statistics in fully developed channel flow at low Reynolds number", *J. Fluid Mech*, Vol. 177, pp. 133-166.

Launder B. E., Reece G. C., Rodi W.: 1975, "Progress in the development of a Reynolds-stress turbulence closure", *J. Fluid Mech*, Vol. 68, pp. 537-566.

Oberlack, M., 1997, "Unified Theory for Symmetries in Plane Parallel Turbulent Shear Flows", *Manuscript no. 163*, Center for Turbulence Research, NASA Ames/Stanford Univ., under review in *J. Fluid Mech.*

Oberlack, M., Cabot, W. & Rogers, M. M., 1998, "Group analysis, DNS and modeling of a turbulent channel flow with streamwise rotation", *Center for Turbulence Research Summer Program*, pp. 221-242.

Speziale C. G., Sarkar S., Gatski T., 1991, "Modelling the pressure-strain correlation of turbulence: an invariant dynamical system approach", *J. Fluid Mech.*, Vol. 227, pp. 245-272.